Mon. Not. R. Astron. Soc. **000**, 000–000 (2001) Printed 1 February 2008 (MN LATEX style file v2.2)

The Formation of Ultra-Compact Dwarf Galaxies

Michael Fellhauer and Pavel Kroupa
Institute for Theoretical Physics and Astrophysics, University of Kiel, Germany

submitted 10.08.2001 – accepted 26.10.2001

ABSTRACT
Recent spectroscopic observations of galaxies in the Fornax-Cluster reveal nearly unresolved 'star-like' objects with red-shifts appropriate to the Fornax-Cluster. These objects have intrinsic sizes of $\approx$ 100 pc and absolute B-band magnitudes in the range $-14 < \mathrm{M_B} < -11.5$ mag and lower limits for the central surface brightness $\mu_\mathrm{B} \gtrsim 23$ mag/arcsec^2 (Phillipps et al. 2001), and so appear to constitute a new population of ultra-compact dwarf galaxies (UCDs). Such compact dwarfs were predicted to form from the amalgamation of stellar super-clusters (Kroupa 1998), which are rich aggregates of young massive star clusters (YMCs) that can form in collisions between gas-rich galaxies. Here we present the evolution of super-clusters in a tidal field. The YMCs merge on a few super-cluster crossing times. Super-clusters that are initially as concentrated and massive as knot S in the interacting Antennae galaxies (Whitmore et al. 1999) evolve to merger objects that are long-lived and show properties comparable to the newly discovered UCDs. Less massive super-clusters resembling knot 430 in the Antennae may evolve to ω Cen-type systems. Low-concentration super-clusters are disrupted by the tidal field, dispersing their surviving star clusters while the remaining merger objects rapidly evolve into the $\mu_\mathrm{B} - M_\mathrm{B}$ region populated by low-mass Milky-Way dSph satellites.

Key words: galaxies: interactions – galaxies: formation – galaxies: star clusters – galaxies: dwarfs – globular clusters: ω Cen (NGC 5139) – methods: N-body simulations

1 INTRODUCTION

In a recent spectroscopic survey of all objects around NGC 1399 in the Fornax-Cluster, carried out to find all dwarf galaxies, Phillipps et al. (2001) report five ultra-compact dwarf galaxies (UCDs; see also Hilker et al. 1999). These have spectra typical for late-type metal-rich and old stellar populations, are marginally resolved and have red-shifts comparable to the Fornax-Cluster, ruling out either faint background galaxies or foreground stars. The UCDs have intrinsic sizes of around 100 pc, absolute B-band magnitudes of $-14 < \mathrm{M_B} < -11.5$ mag and lower limits (due to failure to resolve their cores) of the central surface-brightness $\mu_\mathrm{B} \gtrsim 23$ mag/arcsec^2. Further analysis of photographic plates show no sign of low-luminosity envelopes around these objects which rules out the possibility that they are nucleated dwarf ellipticals (dE,N) with faint envelopes. Therefore, these objects are either extremely compact dwarf galaxies or extremely large and massive ($10^7 - 10^8\,M_\odot$, assuming $M/L_\mathrm{B} = 3$) star clusters. In the $\mu_\mathrm{B} - M_\mathrm{B}$ diagram they fall in the empty region between 'ordinary' dwarf galaxies and globular clusters (Fig. 1).

High-resolution HST-images of the star forming regions in interacting galaxies like the Antennae (Whitmore et al. 1999; Zhang & Fall 1999) or Stephan's Quintet (Gallagher et al. 2001) resolve some of these regions into dozens to hundreds of young massive star clusters. According to Whitmore et al. the individual clusters have effective radii of about 4 pc and masses 10^4–10^6 $\mathrm{M}_\odot$, with a mass-spectrum following a steep power law $\Psi_M \propto M^{-2}$ (Zhang & Fall 1999). The striking point is that these young star clusters are themselves clustered into groups of a few to several hundred star clusters spanning projected regions of a few 100 pc, with a higher cluster concentration at the centre. Measurements of the relative velocities between the star clusters within such objects are now becoming available. Preliminary results indicate $\approx$ 20 km/s (B. Whitmore, private communication), which is consistent with virial masses $\approx 10^7\,M_\odot$. Age determinations in the Antennae show that these star clusters are extremely young (3–7 Myr). While in the Antennae young massive star clusters are preferably found in the central region of the interacting pair, NGC 7319 in Stephan's Quintet has young star clusters in the long tidal arm and the intragroup region north of NGC 7319 (Gallagher et al. 2001).

Examples of clusters of star clusters are shown in Fig. 1 as thick crosses. Of these, knot "S" is particularly remarkable, as its mass is estimated to be about $2.1 \times 10^7\,M_\odot$ assuming it has a mass-to-light ratio in the photometric V-band of $M/L_\mathrm{V} = 0.076$ for an age of 10 Myr (fig. 7 in Smith & Gallagher 2001) and $M_\mathrm{V} = -15.8$ (section 4.4.2 in Whit-

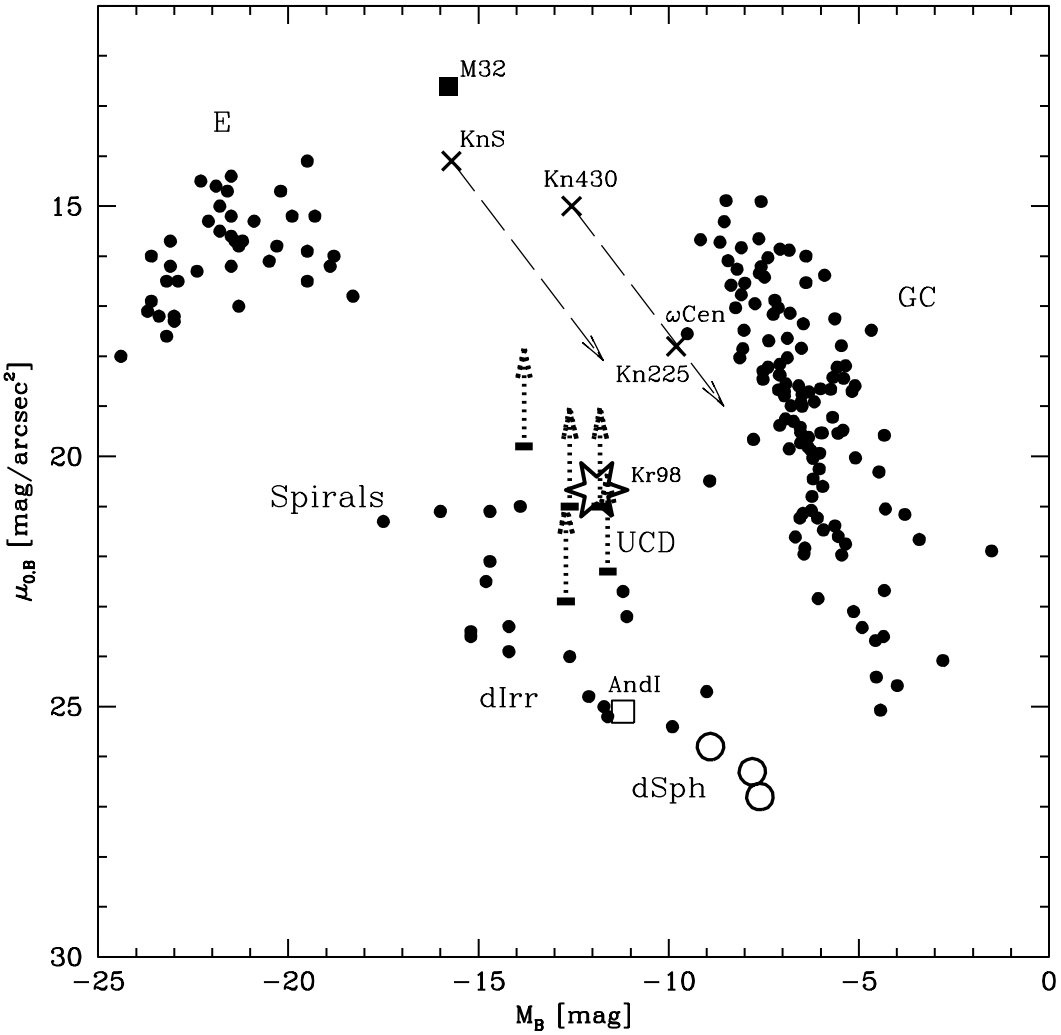

Figure 1. Central surface brightness, $\mu_{0,\mathrm{B}}$, vs absolute photometric B-band magnitude, M_B (the Kormendy diagram). The solid circles are data for Milky-Way globular clusters (GC, Harris 1996), Local-Group dwarf galaxies (dIrr, AndI and dSph, Mateo 1998), elliptical galaxies (E, Peletier et al. 1990). The positions of disk galaxies are indicated by "Spirals" (cf. Ferguson & Binggeli 1994). The newly discovered UCDs are shown by arrows with lower-limits on μ_B (Phillipps et al. 2001). Three "knots", (KnS, Kn430, Kn225, tables 1 and 2 in Whitmore et al. 1999), observed in the interacting Antennae galaxies are shown as thick crosses. Knots KnS and Kn430 are roughly 10 Myr old so that $M/L_\mathrm{V} \approx 0.076$ (fig. 7 in Smith & Gallagher 2001), while Kn225 is about 500 Myr old. The fading of all three knots to $M/L_\mathrm{B} = 3$ due to stellar evolution but assuming no morphological evolution (eq. 1), is indicated by the dashed arrows. The thick six-pointed star shows the merged super-clusters predicted by Kroupa (1998) to result from the dynamical evolution of such knots, which consist of dozens to hundreds of young star clusters.

more et al. 1999). Two other knots (Kn430 and Kn225) are plotted in Fig. 1 with fading vectors to $M/L_\mathrm{B} = 3$ to indicate their position after a few Gyr if the shape of their density profile remains unchanged,

$$\frac{L_\mathrm{c}}{L_\mathrm{tot}} \quad = \quad \text{constant}, \qquad (1)$$

where L_c and L_tot are the central and integrated luminosity, respectively.

The dynamical evolution of these knots is an interesting problem to consider because the merging of many star clusters is not well understood but is a pre-requisite for the understanding of the future fate of such knots. By scaling the numerical results of Garijo, Athanassoula & Garcia-Gomez (1997, hereinafter GAG), who studied the formation of cD galaxies from clusters of 50 equal-mass galaxies, to the present problem of a super-cluster containing 50 star clusters, each cluster having a mass $M_\mathrm{cl} = 10^6\,M_\odot$, Kroupa (1998) studied the dynamical evolution of such "stellar super-clusters". These are not to be confused with the commonly-used terminology 'super-star-cluster', SSC, which is one young star cluster with a mass typical for globular clusters (e.g. Smith & Gallagher 2001). Depending on the initial concentration of such an object, the majority of

star-clusters merge within a few super-cluster crossing times. Within 100 Myr a stellar system forms which has a relaxation time significantly longer than a Hubble time. It is thus a low-mass spheroidal dwarf galaxy (as opposed to the well-known dwarf-spheroidal satellite galaxies, denoted dSph), with a half-mass radius of between about 45 to 100 pc, possibly with a high specific frequency of globular clusters if some survive the merging phase. From figs. 16-18 in GAG the central surface density for essentially all models (collapsing super-clusters and super-clusters initially in virial equilibrium) is 1 mass-unit/length-unit^2. This translates to $\mu = 1000\,M_\odot/\mathrm{pc}^2$ and to the apparent-magnitude surface brightness $\mu_\mathrm{B} = 19.48$ mag/arcsec^2 using

$$\mu_\mathrm{B}[\mathrm{mag/arcsec}^2] = -2.5\log_{10}\left(\mu\,\frac{L_\mathrm{B}}{M}\right) + M_{\mathrm{B},\odot} - 5 + \mathcal{S}, \quad (2)$$

where $M_{\mathrm{B},\odot} = +5.41$ is the absolute B-band magnitude of the Sun, and $\mathcal{S} = 26.572 = 2.5\log_{10} f^2$ with $f = 2.06 \times 10^5$ arcsec per radian, and assuming the B-band mass-to-light ratio $M/L_\mathrm{B} = 3$ in solar units. Assuming that 50–100 per cent of all clusters merge to form the spheroidal dwarf galaxy, its integrated absolute B-band magnitude,

$$M_\mathrm{B} = -2.5\log_{10}\left(M\,\frac{L_\mathrm{B}}{M}\right) + M_{\mathrm{B},\odot}, \quad (3)$$

where M is the mass of the object in $M_\odot$, lies in the range $-12.64 \leq M_\mathrm{B} \leq -11.89$.

Fig. 1 shows that the predicted spheroidal dwarf galaxies fall in the region of the Kormendy diagram that the UCD data of Phillipps et al. (2001) cover, nicely verifying the prediction. The hypothesis that the UCDs were formed as super-clusters appears to be a reasonable possibility, since gas-rich galaxies will have merged in profusion in sub-groups during the early phases of the formation of the Fornax galaxy cluster. The UCDs may thus have formed during the coalescence of a subgroup of late-type gas-rich galaxies, which was infalling into the Fornax cluster. Tidal shocking of such UCDs and/or initially less-massive super-clusters may account for some if not the majority of known spheroidal dwarf galaxies found in large numbers in rich galaxy clusters (Gallagher, Conselice & Wyse 2001).

Kroupa (1998) studied isolated super-clusters, but tidal shaping of the merger objects may be significant. In this contribution we report self-consistent stellar-dynamical calculations of the merging process in super-clusters whilst they are immersed in the tidal field of a parent galaxy. A detailed study of the merging time-scales and efficiencies for super-clusters on circular orbits shows that the star clusters merge very efficiently on a few dynamical time-scales of the super-cluster (Fellhauer et al. 2001). In this paper we focus on a comparison with the recently discovered UCDs and perform computations of super-clusters with varying initial concentrations on eccentric orbits.

The models are explained in Sect. 2 where a brief description of the N-Body code is given. In Sect. 3 the properties of the merger objects on circular orbits are briefly described and a model on an eccentric orbit is discussed in detail. The evolution of a low-mass extended merger object is also studied. Conclusions are presented in Section 4.

2 NUMERICAL METHOD AND SETUP

2.1 The code

The orbital integration of the particles is performed with the particle-mesh code SUPERBOX (Fellhauer et al. 2000). In SUPERBOX densities are derived on Cartesian grids using the nearest-grid-point (NGP) scheme. From these density arrays the potential is calculated via the fast Fourier-transformation. Forces are obtained using higher-order differentiation based on the NGP scheme but comparable in precision with standard CIC (cloud-in-cell) algorithms. The particles are integrated using a fixed time-step Leap-Frog algorithm. For an improved resolution at the regions of interest, a hierarchical grid-architecture with two levels of high resolution sub-grids are used for each star cluster in the super-cluster. These sub-grids track the density maxima of the individual star clusters, and are adjusted at the beginning of the computation to meet individual requirements.

The sizes of the two high resolution grid-levels are chosen such that the innermost grids with the highest resolution (1 pc per grid-cell length) cover the star clusters, while the medium-resolution grids cover the merger object to ensure that the forces between each cluster are treated at least at medium resolution. Finally, the outermost grid, which stays fixed and has the lowest resolution, covers the whole orbit of the super-cluster around the parent galaxy. The time-step used in the calculations is $dt = 0.1$ Myr, which is significantly shorter than the crossing time in the star-clusters ($t_\mathrm{cr} \approx 6$ Myr).

Out notation is as follows: we use large letters for galactocentric coordinates (X, Y, Z, R) and derived quantities, and small letters (x, y, z, r) for super-cluster-centric coordinates and derived quantities.

2.2 Orbits

The super-cluster orbits within an external potential of a parent galaxy given by

$$\Phi(R) = \frac{1}{2}V_0^2 \cdot \ln(R_\mathrm{gal}^2 + R^2) \quad (4)$$

with core radius $R_\mathrm{gal} = 4$ kpc and circular velocity $V_0 = 220$ km/s. Dynamical friction is also analytically added using the Chandrasekhar expression (Binney & Tremaine, their eq. 7-18):

$$\frac{\mathrm{d}\vec{V}_M}{\mathrm{d}t} = -\frac{4\pi\ln(\Lambda)G^2\varrho_\mathrm{gal}M_\mathrm{sc}}{V_M^3} \times \left[\mathrm{erf}\left(\frac{V_m}{\sqrt{2}\sigma}\right) - \frac{\sqrt{2}V_M}{\sqrt{\pi}\sigma}\exp\left(-\frac{V_M}{\sqrt{2}\sigma}\right)\right]\cdot\vec{V}_M \quad (5)$$

with $\ln(\Lambda) = 1.5$ (Velazquez & White 1999; Fellhauer et al. 2000) the so-called Coulomb-logarithm, ϱ_gal is the density of the galactic halo at the position of the super-cluster, M_sc is the total mass of the super-cluster, V_M is the orbital velocity of the super-cluster in the tidal field of the host galaxy and σ is the velocity dispersion in the galactic halo at the position of the super-cluster.

We adopt the tidal field of a Milky-Way type galaxy, but our results are applicable to a galaxy cluster such as Fornax in the sense that super-clusters that remain stable over many highly eccentric orbits will also survive in the potential

Table 1. Properties and orbits of the model super-clusters. The columns give the following data: name of the model, number of star clusters in the super-cluster, Plummer-radius of the super-cluster, crossing time of the super-cluster, total mass of the super-cluster, perigalacticon distance, apo-galacticon distance, orbital period, concentration parameter, strength of tidal field parameter.

name	N_0	$r_{\rm pl}^{\rm sc}$ [pc]	$t_{\rm cr}^{\rm sc}$ [Myr]	$M_{\rm sc}$ [$10^7 {\rm M}_\odot$]	$R_{\rm peri}$ [kpc]	$R_{\rm apo}$ [kpc]	$T_{\rm orb}$ [Myr]	α	$\beta_{\rm peri}$
SD05A	20	50	7.4	2.0	10	10	300.7	0.12	0.62
SD06A	20	75	13.5	2.0	10	10	300.7	0.08	0.93
SD09A	20	50	7.4	2.0	20	20	569.6	0.12	0.42
SD10A	20	75	13.5	2.0	20	20	569.6	0.08	0.60
SD11	20	150	38.3	2.0	20	20	569.6	0.04	1.28
SD17B	20	50	7.4	2.0	50	50	1400.7	0.12	0.23
SD18A	20	75	13.5	2.0	50	50	1400.7	0.08	0.35
SD19E	20	150	38.3	2.0	50	50	1400.7	0.04	0.70
R06	20	300	108.4	2.0	30	60	900	0.02	2.0
E01	32	50	9.4	1.2	2	20	250	0.08	1.29

well of Fornax, whereas super-clusters that are torn apart immediately are not likely to survive in a galaxy cluster. Gallagher, Conselice & Wyse (2001) discuss dwarf-galaxy survival in more detail, and we note that spheroidal dwarfs without dark matter can readily survive passages through the centres of galaxy-clusters owing to the large encounter velocities. We do not aim to model the UCDs observed in the Fornax cluster in detail, which is impossible in any case given that little is known about their orbits, but merely concentrate on the generic properties of the merger objects when they are subject tidal fields that vary in strength.

To study the merging time-scales and efficiencies circular orbits are adopted where the centre of the super-cluster is placed at a distance $R = D$ from the galactic centre. The distance D is varied in the range of 5–100 kpc. A detailed discussion of the involved time-scales can be found in Fellhauer et al. (2001). To study the evolution of the merger objects in a time-dependent tidal field the parameter space is extended to eccentric orbits.

2.3 Super-clusters

A range of models (Table 1) are setup to investigate the importance of the tidal field and initial concentration of the super-cluster.

The young massive star clusters are modelled as Plummer-spheres with Plummer-radii $r_{\rm pl}$ = 4–6 pc and cut-off radii 20–30 pc. The clusters all have masses of 10^6 $\rm M_\odot$ if no mass spectrum is taken into account, or 10^6 $\rm M_\odot$ and $3.2 \cdot 10^5$ $\rm M_\odot$ to model a mass spectrum. Estimating the relaxation time $t_{\rm relax}$ of these star clusters (Spitzer & Hart 1971),

$$t_{\rm relax} = 0.138 \cdot \frac{\sqrt{M_{\rm cl}} r_h^{3/2}}{\langle m \rangle \sqrt{G} \ln(0.4\, n)}. \quad (6)$$

where $M_{\rm cl}$ is the mass of the star cluster, r_h is the half-mass radius, the average stellar mass $\langle m \rangle = 0.4$ $\rm M_\odot$ (using the universal IMF, Kroupa 2001) and n the number of stars. This leads to $t_{\rm relax} \approx$4 Gyr for the more massive star clusters and 2.5 Gyr for the less massive ones. These time-scales are much longer than the cluster–cluster merging time-scale. The resulting merger objects have relaxation times longer than a Hubble time. Surviving star clusters are only counted and their position is traced; their internal evolution is not studied here. Therefore it is possible to carry out the orbital integration with a particle-mesh code which suppresses two-body relaxation processes.

To model a super-cluster, N_0, of these clusters are placed in a Plummer distribution with Plummer radius ($r_{\rm pl}^{\rm sc}$) ranging from 50–300 pc and cut-off radius ($r_{\rm cut}^{\rm sc}$). The super-cluster is initially in virial equilibrium.

To describe our parameters with dimensionless variables we define

$$\alpha = r_{\rm pl}/r_{\rm pl}^{\rm sc}, \quad (7)$$

$$\beta = r_{\rm cut}^{\rm sc}/r_{\rm tidal}, \quad (8)$$

where $r_{\rm tidal}$ is the tidal radius of the super-cluster. In the case of eccentric orbits the tidal radius is estimated at perigalacticon,

$$r_{\rm tidal} = \left(\frac{M_{\rm sc}}{3\, M_{\rm gal}(R)} \right)^{1/3} R_{\rm peri}. \quad (9)$$

While α describes how densely the super-cluster is filled with star clusters, β indicates the strength of the tidal forces acting on the super-cluster. With our choices of the parameters $r_{\rm pl}^{\rm sc}$ and D, α ranges from 0.02 to 0.12 and β falls in the interval 0.2 to 2.7.

The relaxation time of the cluster system is very short, i.e. using Eq. 6 with $n = N_0$ would lead to a nominally shorter relaxation time than the crossing time of the super-clusters (about 0.3–0.4 $t_{\rm cr}^{\rm sc}$). This shows that such systems are heavily collision-dominated and therefore the merging process is violent and the merging timescales should be very short.

3 RESULTS

As discussed by Kroupa (1998) and Fellhauer et al. (2001) the evolution of the young super-cluster is dominated initially, during the violent merging time, by cluster–cluster

Table 2. Sizes of the merger objects, measured at $t = 1$ Gyr and at $t = 5$ Gyr for different choices of α and β. Only the bound mass is taken into account (cf. Fig. 4).

name	α	β	Half-Mass Radius [pc]		90 %-Mass Radius [pc]		Tidal Radius [pc]	
			$t = 1.0$ Gyr	$t = 5.0$ Gyr	$t = 1.0$ Gyr	$t = 5.0$ Gyr	$t = 1.0$ Gyr	$t = 5.0$ Gyr
SD05A	0.12	0.62	39.0	40.5	123.2	135.4	400	400
SD06A	0.12	0.42	48.0	50.2	151.5	150.9	600	600
SD09A	0.12	0.23	38.3	39.0	125.5	124.2	1,120	1,120
SD10A	0.08	0.93	79.2	77.3	200.0	188.9	390	390
SD11	0.08	0.60	43.0	44.5	146.1	150.9	610	610
SD17B	0.08	0.35	71.2	72.4	230.4	221.5	1,110	1,110
SD18A	0.04	1.28	181.2	144.6	491.1	348.1	580	580
SD19E	0.04	0.70	236.6	163.2	1,058.8	576.5	1,010	910
R06	0.02	2.00	—	—	—	—	—	—
E01	0.08	1.29	54.6	41.9	149.2	146.3	188	152

merging and interaction processes. The merging efficiency is, in general, very high. As long as the cutoff radius is smaller than the tidal radius ($\beta \leq 1.0$) almost all star clusters merge. The total number of clusters that merge decreases linearly and slowly with increasing $\beta > 1$.

3.1 Circular orbits

The merger objects consisting initially of $N_0 = 20$ massive star clusters (each with 10^6 $M_\odot$) on circular orbits have half-mass radii and sizes summarised in Table 2. The time-scale for the merging process is very short. Within $5 - 10 \times t_{\rm cr}^{\rm sc}$ ($t_{\rm cr}^{\rm sc}$ being the internal crossing time of the super-cluster) the initial violent merging phase is over. During this phase the number of remaining clusters decreases exponentially, the decay thus being similar to the radioactive decay law. For initially concentrated super-clusters ($\alpha \geq 0.08$) this phase lasts $\lesssim$100 Myr. The resulting merger object is very dense and stable over 10 Gyr. In Fig. 1 it coincides with the Kr98 prediction.

As long as $0.08 \lesssim \alpha \lesssim 0.12$ there is almost no evolution in mass and size of the merger object. If $\alpha \lesssim 0.04$ or $\beta > 1.0$ the merger object looses a part of its mass and shrinks until it reaches a stable configuration, and is associated with a population of surviving star clusters that spread out along the orbit. The merger object lies close to the Kr98 prediction in Fig. 1 despite the mass lost.

Between 70 and 95 % of the mass of the super-cluster ends up in the merger objects, which have central densities of about 650 $M_\odot/{\rm pc}^3$ and exponential scale lengths of about 9 pc. The surface density can be well fitted by a de-Vaucouleur-profile, the line-of-sight velocity dispersion is about 20 km/s. The shape of the objects is spherical with axes-ratios larger than 0.9.

3.2 Dense super-cluster on an eccentric orbit

The models are extended to include eccentric orbits to study the influence of tidal heating acting on the super-clusters and the resulting merger objects (Table 1). As reference model in this paper we start with a dense super-cluster containing $N_0 = 32$ star clusters, 3 having a mass of 10^6 $M_\odot$ and 29 having $3.2 \cdot 10^5$ $M_\odot$ to mimic a mass spectrum of the form $\Psi_M \propto M^{-2}$. The star clusters have a Plummer radius of $r_{\rm pl} = 4$ pc and crossing times of 0.75 and 1.32 Myr, respectively. The super-cluster they are distributed in, has a total mass $M_{\rm sc} = 1.23 \times 10^7$ $M_\odot$, a Plummer radius $r_{\rm pl}^{\rm sc} = 50$ pc, a cut-off radius of $r_{\rm cut}^{\rm sc} = 250$ pc (giving $\alpha = 0.08$) and a crossing time of 9.4 Myr. The super-cluster is placed at apo-galacticon ($D = 20$ kpc) on a highly eccentric orbit with eccentricity $e = 0.82$, where

$$e = \frac{R_{\rm apo} - R_{\rm peri}}{R_{\rm apo} + R_{\rm peri}}. \quad (10)$$

At perigalacticon $\beta_{\rm peri} = \beta = 1.29$. However, since the orbit starts at apo-galacticon and has an orbital period $T_{\rm orb} \approx 250$ Myr the super-cluster has $\beta < 1$ for a time-span $n_t \times t_{\rm cr}^{\rm sc}$, $n_t \approx 10$, giving enough time for the super-cluster to evolve essentially as the models studied above. Most star clusters merge within $5 \times t_{\rm cr}^{\rm sc}$ (Fig. 2). The number of star clusters decreases exponentially,

$$N(t) = N_0 \cdot \exp\left(-\frac{t}{\tau}\right), \quad (11)$$

with t measured in units of the crossing time of the super-cluster and $\tau = 5\, t_{\rm cr}^{\rm sc}$ which corresponds to 47 Myr for model E01. This exponential decrease is shown as a straight line in Fig. 2. The initial violent merging phase is dominated by clusters on highly eccentric orbits within the super-cluster. Star clusters initially on near-circular orbits in the super-cluster survive until $\gtrsim 5\, t_{\rm cr}^{\rm sc}$, but ultimately they merge due to dynamical friction within the super-cluster.

The mass of the merger object is $M_{\rm mo} = 1.12 \cdot 10^7$ $M_\odot$ which corresponds to 91.5% of the total mass of the super-cluster. The remaining mass is lost due to internal heating from cluster–cluster collisions and subsequent loss due to the tide. The mass of the merger object decreases with every perigalacticon passage. The averaged mass-loss rate is $5.7 \cdot 10^5$ $M_\odot$/Gyr. After 10 Gyr the total mass of the remaining object is $0.59 \cdot 10^7$ $M_\odot$.

By $t = 1$ Gyr, the gravitationally bound particles comprising the merger object have a diameter of several 100 pc with an elliptical envelope ($\varepsilon \approx 0.6$) but a spherical and very dense core (Fig. 3). Bound particles have negative binding energies relative to the merger object. The half-mass radius

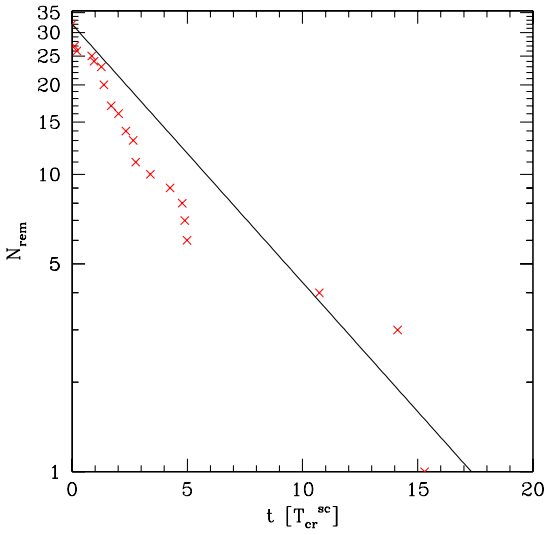

Figure 2. The number of remaining star clusters, $N_{\rm rem}$, vs. time for model E01. Within the first 5 crossing times of the super-cluster the merging can be fitted with an exponential with an exponential decay time of about 47 Myr. This is the same fit as already obtained by Fellhauer et al. (2001) for a large variety of super-clusters.

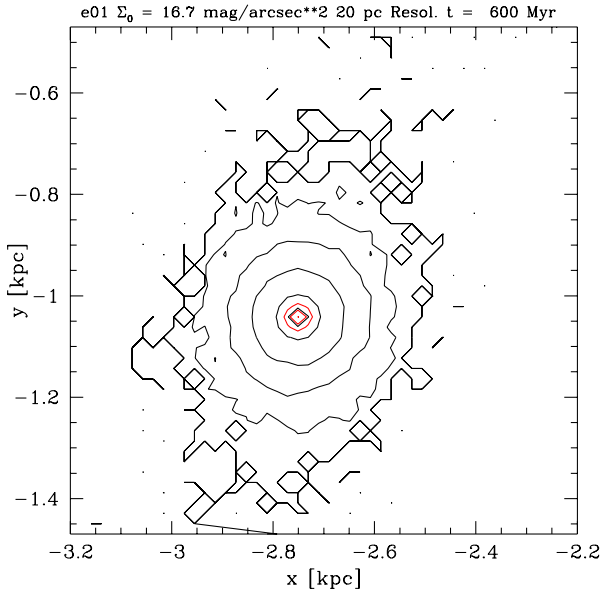

Figure 3. Contour plot of the merger object E01 at 600 Myr shortly after the violent merging phase is over. While the central area is circular, the envelope shows an ellipticity of about 0.6.

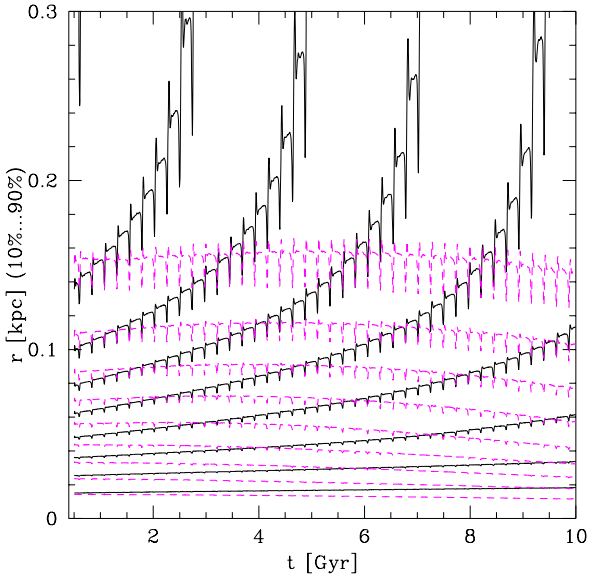

Figure 4. Lagrangian radii containing 10, 20, ..., 90 % of the mass of merger object E01 vs. time. Solid lines are all particles, dashed lines are the bound particles only.

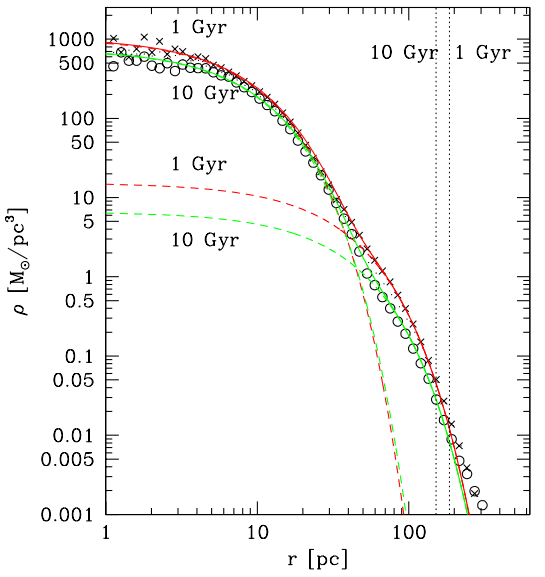

Figure 5. Radial density profile of merger object E01 at $t = 1$ (crosses), 5 (points) and 10 Gyr (circles). Profiles can be fitted by two exponentials (dashed lines, according to eq. 12) with the overall fitting function as solid line. Vertical lines show the tidal radii at $t = 1$ and 10 Gyr derived from Eq. 9.

$r_{\rm h} = 54.6$ pc and $r(90\%) = 149.2$ pc holds 90 % of the mass (Fig. 4). Examining the surface density profile (Fig. 6), the core radius $r_{\rm core} = 10$ pc (the radius where the surface density drops to half the central value). The tidal radius at perigalacticon, estimated from Eq. 9 is $r_{\rm tidal} \approx 188$ pc. The morphology of the object stays almost constant during the whole computation time. At $t = 10$ Gyr the half-mass radius is $r_h = r(50\%) = 41.9$ pc, $r(90\%) = 146.3$ pc, $r_{\rm core} = 9.5$ pc and $r_{\rm tidal} = 152$ pc, as shown in Fig. 4.

The structure of the merger object (MO) can be best fitted by a double exponential profile. The MO shows a very dense core surrounded by an exponential envelope. Defining

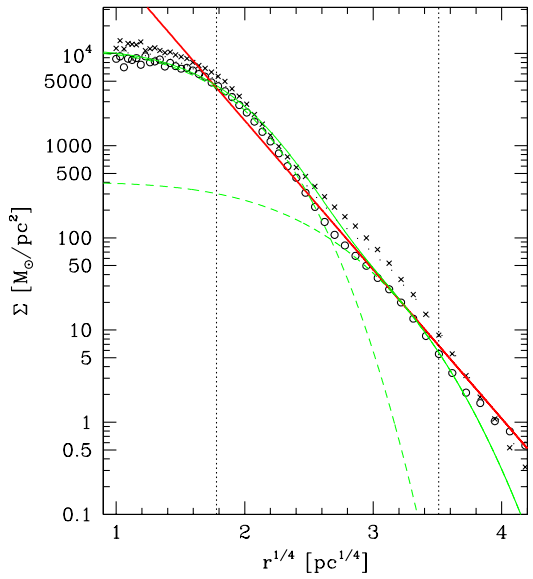

Figure 6. Surface density profile of the merger object E01. Profiles are displayed at $t = 1$ (crosses), 5 (dots), 10 Gyr (circles). Solid thick line shows a de-Vaucouleurs fit to the data at $t = 10$ Gyr. Also shown as dashed lines are two exponentials as a fitting function with the sum of both shown as thin solid curve. Right vertical dotted line shows the tidal radius taken from Eq. 9, left vertical dotted line shows the core radius (both at $t = 10$ Gyr).

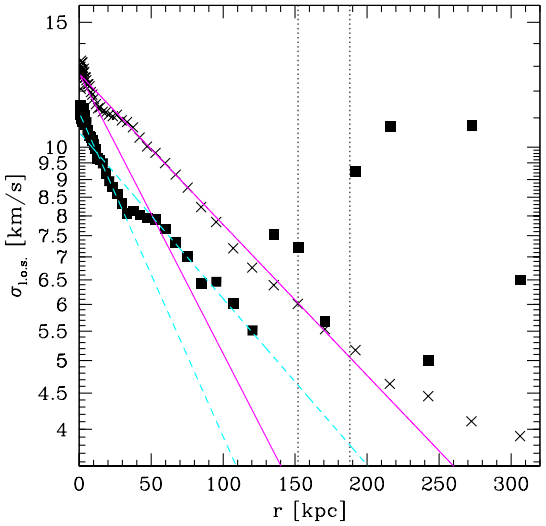

Figure 7. Line-of-sight velocity dispersion profiles of merger object E01 at $t = 1$ (crosses) and 10 Gyr (boxes). Profiles can be fitted by exponentials. Fitting parameters for $t = 1$ Gyr: inner: $\sigma_0 = 12.7 \pm 0.1$ km/s, $r_{\rm exp} = 110 \pm 10$ pc; outer: $\sigma_0 = 12.4 \pm 0.2$ km/s, $r_{\rm exp} = 222 \pm 5$ pc; $t = 10$ Gyr: inner $\sigma_0 = 11.6 \pm 0.6$ km/s, $r_{\rm exp} = 90 \pm 2$ pc; outer: $\sigma_0 = 10.5 \pm 0.3$ km/s, $r_{\rm exp} = 185 \pm 10$ pc.

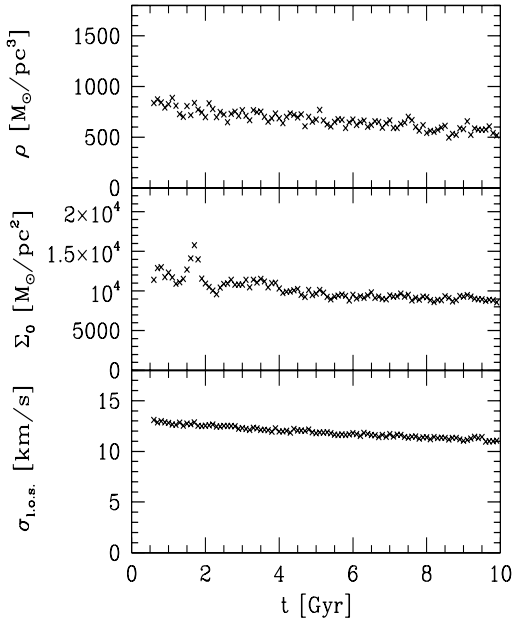

Figure 8. Time evolution of the central values of space density, surface density and line-of-sight velocity dispersion of merger object E01.

the profile as

$$\rho(r) \quad = \quad \rho_0 \, \exp\left(-\frac{r}{r_{\rm exp}}\right), \tag{12}$$

the central density at $t = 1$ Gyr is $\varrho_0 = 1030 \pm 40$ M$_\odot$/pc^3 and the exponential scale length of the core is $r_{\rm exp} = 6.7 \pm 0.2$ pc. The envelope has $\varrho_0 = 15.3 \pm 0.7$ M$_\odot$/pc^3 and $r_{\rm exp} = 26.0 \pm 0.3$ pc. After 10 Gyr the values change to $\varrho_0 = 750 \pm 15$ M$_\odot$/pc^3 and $r_{\rm exp} = 7.1 \pm 0.1$ pc for the core and $\varrho_0 = 6.6 \pm 0.5$ M$_\odot$/pc^3 and $r_{\rm exp} = 27.8 \pm 0.8$ pc for the envelope. Fig. 5 shows the data points for $t = 1$, 5 and 10 Gyr and the fitted functions for $t = 1$ and 10 Gyr. Plotted as vertical lines are the approximate tidal radii (Eq. 9). The tidal extension of the MO beyond the tidal radius is clearly evident.

The surface density is well fitted by a single de-Vaucouleur profile,

$$\Sigma(r) \quad = \quad \Sigma_{\rm v} \cdot \exp\left(-7.67\left[\left(\frac{r}{r_{\rm v}}\right)^{1/4} - 1\right]\right), \tag{13}$$

with $\Sigma_{\rm v} = 1500$ M$_\odot$/pc^2 and $r_{\rm v} = 18$ pc (fitted at $t = 1$ Gyr) (Fig. 6). Fitting the profile at $t = 10$ Gyr with two exponentials, results in a central surface density of 10600 ± 300 M$_\odot$/pc^2 and exponential scale lengths of 10.8 ± 0.4 and 35.7 ± 0.5 pc, respectively.

Measuring the line-of-sight velocity dispersion shows that the central velocity dispersion is about 13 km/s at the beginning and drops down to about 11 km/s after 10 Gyr. The velocity dispersion profile can be fitted by two exponentials (Fig. 7).

The central density, surface density and velocity dispersion decrease only very slowly and linearly with time

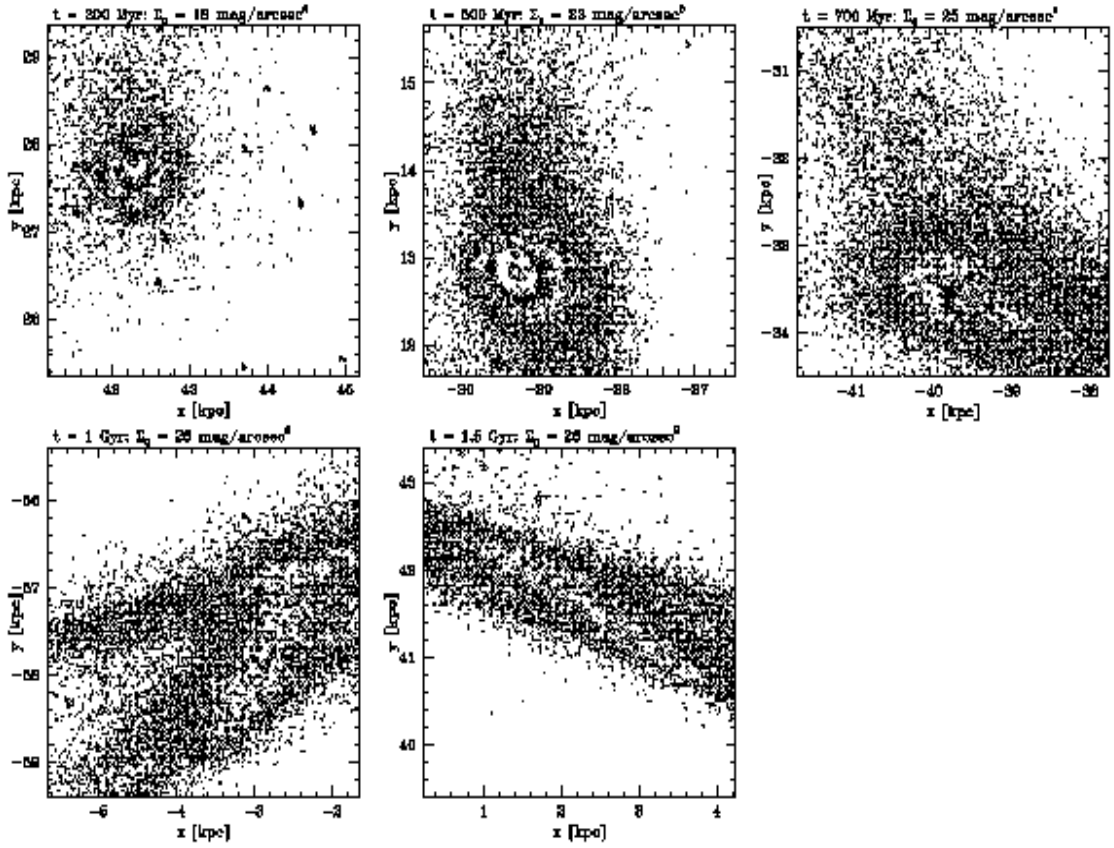

Figure 9. Evolution and destruction of the low-mass merger object R06. Shown are contour-plots with 20 pc resolution. Snapshots are at $t = 200$, 500, 700, 1000 and 1500 Myr. Highest surface-brightness (adopting $M/L = 1$) of the MO is indicated above each panel.

(Fig. 8). The merger object is thus massive and stable enough to survive for a Hubble time despite the very large orbital eccentricity.

3.3 Low-concentration super-cluster on an eccentric orbit

If the initial super-cluster has a sufficiently small α and is subject to a strong tidal field, the merging efficiency can be low. The resulting merger object has a smaller mass and is less concentrated than model E01 above. Merger objects like this are easily disrupted at their first perigalacticon passage forming an unbound stream of stars and surviving star clusters moving along almost identical orbits. However, a density enhancement survives for a substantial time, being composed of a core of particles with similar phase-space coordinates that may perhaps be identified as a dSph satellite (Kroupa 1997; Klessen & Kroupa 1998).

In a calculation of a model with a Plummer radius of the super-cluster of 300 pc orbiting on an eccentric orbit with $e = 0.33$ only a small merger object R06, made out of 4 star clusters, forms. It has a mass of about $0.35 \cdot 10^7$ $M_\odot$ and gets dissolved after the first perigalacticon passage (Fig. 9). The 'central' density drops from 100 $M_\odot/pc^3$ down to 0.01 $M_\odot/pc^3$. The stars of this density enhancement cover an area a few kpc in diameter. Despite the fact that the stars do not form a bound entity, the density enhancement is still detectable after a few Gyrs.

3.4 Evolution in the Kormendy diagram

The models discussed in Sections 3.1-3.3 are placed in the Kormendy diagram for a comparison with known stellar systems (Fig. 10).

The models on circular orbits (Section 3.1) overlap the Kr98 prediction shown as the six-pointed open star assuming $M/L_B = 3$. These models do not evolve noticeably over a Hubble time, apart from slight fading due to stellar evolution.

The evolution of the dense super-cluster on a highly eccentric orbit (Section 3.2) is shown for ages between 600 Myr and 10 Gyr as the solid curve in the thick box labelled E01. Again, the evolution due to tidal harassment is not significant. The position of the equivalent 5 Myr old stellar cluster with $R_{Pl} = 50$ pc and $M = 1.23 \times 10^7\, M_\odot$ is shown as the upper thick dotted open square labelled with the mass-to-light ratio $M/L_B = 0.0144$ (fig. 7 in Smith & Gallagher 2001) and assuming $B - V = 0$. Fading without morphological evolution (Eq. 1) to $M/L_B = 3$ places such a cluster at the end of the thick long-dashed arrow in the vicinity of the Kr98 prediction, while the actual evolution (photometric and dynamical) places it in the open box which lies in the vicinity of the fading vector of knot S (thick cross).

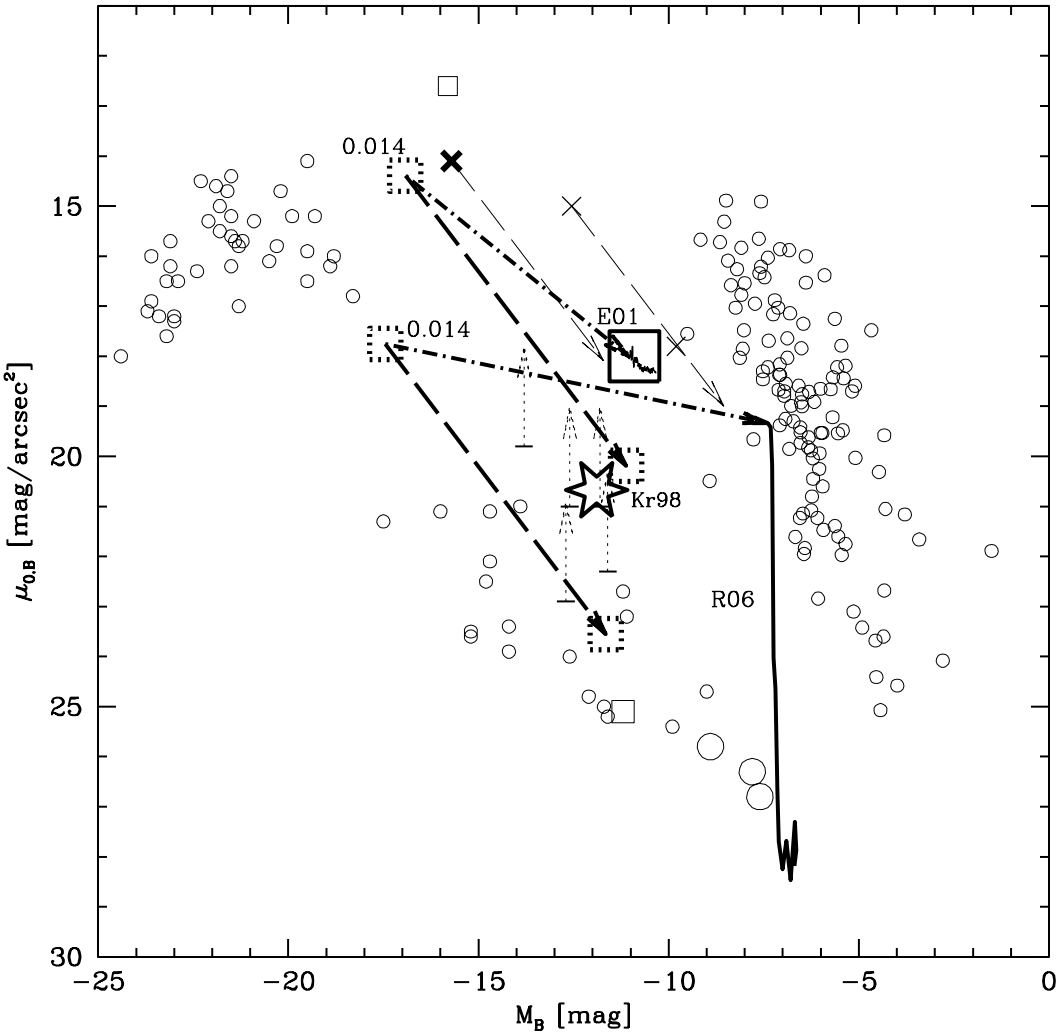

Figure 10. Known stellar systems are shown as faint open symbols, apart from highlighted knot S (Fig. 1). Models E01 and R06 are shown at an age of about 5 Myr as the thick dotted squares assuming $M/L_{\rm B} = 0.014$. Fading without morphological evolution to $M/L_{\rm B} = 3$ would place these at the tips of the thick long-dashed arrows. The actual dynamical evolution is plotted as solid curves assuming the merger objects have $M/L_{\rm B} = 3$.

The evolution of the low-density super-cluster on an eccentric orbit (Section 3.3) is shown for ages spanning from 200 Myr to 1.5 Gyr as the thick solid line labelled R06. By 1.5 Gyr a remnant object stabilises in the vicinity of the known dSph satellites, and sports a population of 16 co-streaming globular clusters. An equivalent stellar system that has the same Plummer density profile and mass as the initial super-cluster R06 appears at an age of about 5 Myr at the position of the lower thick dotted box labelled as $M/L_{\rm B} = 0.014$. It would resemble a low-mass dIrr, since the distribution of brilliant young star clusters would appear patchy in such a system. Hunter, Hunsberger & Roye (2000) discuss observable signatures of tidal-dwarf galaxies which may be related to this class of object. Fading to $M/L_{\rm B} = 3$ without morphological evolution would place this object at the end of the thick long-dashed arrow, in the vicinity of bright dSph satellites.

Finally, from Fig. 1 we note that knot 430 (age $\approx$ 10 Myr), which is less massive than S but has a similar central surface density, may evolve via fading slightly past knot 225 (age $\approx$ 500 Myr) to $M/L_{\rm B} = 3$ if it undergoes no morphological evolution (eqn 1). Since the Milky-Way globular cluster ω Cen also lies in the vicinity of the final position of faded knot 430, we may assume that the precursor of ω Cen may have looked similar to knot 430, or an object even more massive lying closer to knot S if dynamical evolution is taken account of (Fig. 10). ω Cen may thus have been born as a super-cluster containing hundreds of star clusters. Such a scenario may also be consistent with the unusual metallicity distribution in ω Cen (e.g. Smith et al. 2000), which is being taken as evidence that this unusual

cluster may in fact be a compact dwarf galaxy. Such an object encompassing about one hundred pc most probably forms over 5-10 Myr (Elmegreen et al. 2000) so that self-enrichment through supernovae is very likely. This scenario merits further study.

4 CONCLUSIONS

When gas-rich galaxies interact strongly the supersonically colliding gas clouds are pressurised to such an extend that they profusely form stars in super-clusters that have masses ranging from 10^7 to $10^8\,M_\odot$ and dimensions of a few hundred pc. Such sub-structures are observed to form in tidal arms in computer models of colliding galaxies (Barnes & Hernquist 1992; Elmegreen, Kaufman & Thomasson 1993), and are also evident in high-resolution HST images of the Antennae galaxies (Whitmore et al. 1999).

These reveal the super-clusters to be composed of many star-clusters, thus essentially conforming to the hierarchical star-formation picture discussed by Elmegreen et al. (2000), according to which sub-structure exists on every scale. This is evident in local embedded clusters (Megeath et al. 1996; Kaas & Bontemps 2001) as well as the region with a radius of a few hundred pc around 30 Dor in the Large Magellanic Cloud, which contains many star clusters smaller and less massive than the central cluster R136.

It is thus to be expected that globular clusters will also have formed heavily sub-structured, i.e. essentially composed of many smaller clusters. Extreme cases may lead to ω Cen, which can be interpreted to form the borderline between massive star clusters and small dwarf galaxies. The present findings (Section 3.4) lend credence to this notion, which may also allow an explanation of the metallicity spread in ω Cen.

Even more massive and larger super-clusters, such as are observed for example in the Antennae galaxies (knot S), evolve through a phase of violent star-cluster interactions to stellar systems with relaxation times longer than a Hubble time and so form compact dwarf galaxies that are stable even when subject to strong tides. Examples of such systems may have been discovered recently by Phillipps et al. (2001) in the Fornax galaxy cluster as ultra-compact dwarf galaxies.

Acknowledgements:

MF acknowledges financial support through DFG-grant FE564/1-1. Part of this project (parallelisation of the code and use of high-performance computers) was carried out at the Edinburgh Parallel Computing Centre (EPCC) through the TRACS-programme. The TRACS-programme is a scheme of the European Community: Access to Research Infrastructure action of the Improving Human Potential Programme (contract No. HPRI-1999-CT-00026) which allows young PhD- or post-doctoral scientists to learn parallel computing by offering computing time and support for their projects. MF thanks the staff of EPCC for their support.

REFERENCES

Barnes J.E., Hernquist L., 1992, Nature, **360**, 715
Binney J., Tremaine S., 1987, 'Galactic Dynamics', Princeton University Press
Elmegreen B.G., Kaufman M., Thomasson M., 1993, ApJ, 412, 90
Elmegreen B.G., Efremov Yu.N., Pudritz R.E., Zinnecker H., 2000, in Protostars and Planets IV , eds. V.G. Mannings, A.P. Boss, S.S. Russell (Tucson: Univ. Arizona Press), p.179
Fellhauer M., Kroupa P., Baumgardt H., Bien R., Boily C.M., Spurzem R., Wassmer N., 2000, NewA, **5**, 305
Fellhauer M., Baumgardt H., Kroupa P., Spurzem R., 2001, to appear in Cel. Mech. & Dyn. Astron., astro-ph/0103052
Ferguson H.C., Binggeli B., 1994, A&AR, **6**, 67
Gallagher S.C., Charlton J.C., Hunsberger S.D., Zaritsky D., Whitmore B.C., 2001, AJ, in press (astro-ph/0104005)
Gallagher J.S., Conselice C.J., Wyse R.F.G., 2001, in Dwarf Galaxies and their Environment, eds. K.S. de Boer, R.-J. Dettmar, U. Klein, in press, astro-ph/0108007
Harris W.E., 1996, AJ, **112**, 1487
Hilker M., Infante L., Kissler-Patig M., Richtler T., 1999, A&AS, **134**, 75
Hunter D.A., Hunsberger S.D., Roye E.W., 2000, ApJ, **542**, 137
Kaas A.A., Bontemps S., 2001, in ASP Conf. Ser. Vol. xxx, From Darkness to Light, ed. T. Montmerle & Ph. André (San Francisco: ASP), in press, astro-ph/0008460
Klessen R.S., Kroupa P., (1998) ApJ, **498**, 143
Kroupa P., 1997, NewA, **2**, 139
Kroupa P., 1998, MNRAS, **300**, 200
Kroupa P., 2001, MNRAS, **322**, 231
Mateo M., 1998, ARAA, **36**, 435
Megeath S.T., Herter T., Beichman C., Gautier N., et al., 1996, A&A, 307, 775
Pelletier R.F., Davies R.L., Illingworth G.D., Davies L.E., Cawson M., 1990, AJ, **100**, 1091
Phillipps S., Drinkwater M.J., Gregg M.D., Jones J.B., 2001, to appear in ApJ, astro-ph/0106377
Smith L.J., Gallagher III J.S., 2001, to appear in MNRAS, astro-ph/0104429
Smith V.V., Suntzeff N.B., Cunha K., Gallino R., Busso M., Lambert D.L., Straniero O., 2000, AJ, **119**, 1239
Spitzer L., Hart M.H., 1971, ApJ, **164**, 399
Velazquez H., White S.D.M., 1999, MNRAS, **304**, 254
Whitmore B.C., Zhang Q., Leitherer C., Fall S.M., 1999, AJ, **118**, 1551
Zhang Q., Fall S.M., 1999, ApJL, **527**, 81L